Hierarchical Nanostructuring of Porous Silicon with Electrochemical and Regenerative Electroless Etching

Ermei Mäkilä,[a*] *Anne-Mari Anton Willmore,*[b] *Haibo Yu,*[c†] *Marianna Irri,*[a] *Mark Aindow,*[c]
Tambet Teesalu,[b] *Leigh Trevor Canham,*[d] *Kurt W. Kolasinski,*[e**] *and Jarno Salonen*[a]

[a] Department of Physics and Astronomy, University of Turku, Turku, FI-20014, Finland

[b] Laboratory for Cancer Biology, University of Tartu, Tartu, 50411, Estonia

[c] Department of Materials Science & Engineering, Institute of Materials Science, University of Connecticut, Storrs, CT 06269-3136, USA

[d] School of Physics and Astronomy, University of Birmingham, Birmingham, B15 2TT, United Kingdom

[e] Department of Chemistry, West Chester University, West Chester, PA 19383-2115, USA

ToC Graphic

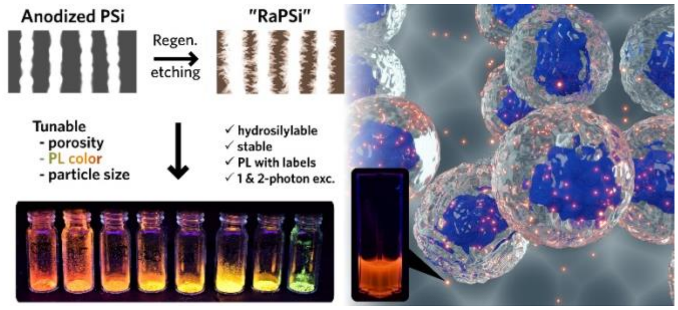

Abstract

Hierarchically nanostructured silicon was produced by regenerative electroless etching (ReEtching) of Si powder made from pulverized anodized porous silicon. This material is characterized by ~15 nm mesopores, into the walls of which tortuous 2–4 nm pores have been introduced. The walls are sufficiently narrow that they support quantum-confined crystallites that are photoluminescent. With suitable parameters, the ReEtching process also provides control over the emission color of the photoluminescence. Ball milling and hydrosilylation of this powder with undecylenic acid produces nanoparticles with hydrodynamic diameter of ~220 nm that exhibit robust and bright luminescence that can be excited with either one ultraviolet/visible photon or two near infrared photons. The long-lived, robust visible photoluminescence of these chemically passivated porous silicon nanoparticles is well-suited for bioimaging and theranostic applications.

Keywords

porous silicon, two-photon fluorescence, photoluminescence, etching, hierarchical nanostructure, nanoparticle

Hierarchically structured silicon holds great promise as a material for applications in theranostics[1, 2] if preparation methods can be found that allow for variation of pore size while still producing pore wall thicknesses that are small enough to facilitate near-infrared (IR) to visible photoluminescence. Bulk silicon is essentially inert in the human body. However, when porosified to produce a more defective, high-surface-area material, it becomes resorbable over practical timescales.[3-5] Porous silicon (PSi) is a biocompatible and biodegradable material,[4] the biological behavior of which can be controlled by porosity and surface chemistry.[6] In the body, it dissolves mainly into silicic acid, which is a bio-available and natural form of Si.[7] A number of synthetic methods are suitable for the modification of PSi surfaces for specific applications.[8-10] This material can also be used as a template for organic and bio-polymers in order to prepare composites with a desired nanostructure.[11-17]

PSi particles have been intensively studied for sustained release of drugs and successfully used to carry a variety of payloads ranging from small molecular drugs[18, 19] to therapeutic biomolecules, such as peptides, siRNA and DNA.[20-24] PSi can also host several different types of drugs simultaneously, for example, a hydrophilic small molecule drug and a hydrophobic peptide,[25] mainly because of the simple and easy drug loading process.[19] The readily modifiable surface chemistry of PSi enables decoration of the particle with target-specific homing peptides for improved payload delivery.[26, 27] It has also been demonstrated that improved blood circulation time and homing efficiency of PSi nanoparticles, which have been modified with polyethylene glycol (PEGylation) and peptide functionalization, are achieved by using ^{111}In labeled undecylenic acid-modified PSi nanoparticles.[28] Homing efficiency can be further refined by antibody-functionalization followed by loading with a chemotherapy drug and gold nanoclusters[29] or by shielding the payload carrying PSi particle with a graphene oxide shell, utilizing the latter also for binding the site-targeting peptide.[30]

Recently, we developed a method known as regenerative electroless etching (ReEtching).[31] This variation of stain etching[32] uses a small amount of one oxidant, such as a V(V) species generated by dissolved V_2O_5, and steady injection of a second oxidant, *e.g.* H_2O_2, with a syringe pump. The V(V) species is believed to be VO_2^+, which is known to couple optimally to the Si valence band for the initiation of etching.[33] Steady injection of H_2O_2 regenerates VO_2^+ and the establishment of a steady-state etch rate that is conducive to deep, homogeneous etching. Coupled with the addition of acetic acid (AcOH) to act as a surfactant that reduces foaming, we demonstrated[31] that unlike previous methods,[34-40] ReEtching is capable of etching powder particles completely without an unetched core. This is important in applications where full biodegradability is required. The ReEtch method is optimized to minimize material loss by limiting the reaction rate through gradual addition of the secondary oxidant, thus keeping the primary oxidant, VO_2^+ amount limited during the etching reaction. Therefore, ReEtching is also more efficient, losing less Si mass to electropolishing while channeling etching into porosification.

Here we demonstrate two additional advantages of ReEtching: it can be used on any Si starting material and the hierarchically porosified product retains bright visible and near-IR photoluminescence (PL). Feedstocks include not only wafers, high-purity granules and metallurgical grade powders, but also PSi powder produced by any other method, *e.g.* magnesiothermal reduction,[41] metal assisted catalytic etching (MACE)[42] or pulverization of anodized wafers.[41, 43] Dosed addition of the secondary oxidant renders the ReEtch process far more controllable than conventional electroless etching. When ReEtching is applied to a porous feedstock, the original pore structure is preserved but also functions as a template for further selective etching. This effectively enables selection of the final porosity of the ReEtched anodized PSi. In addition, the process can be used to considerably increase the specific surface area of the material, to tune the size of the remaining silicon skeleton structure and, thereby, to enhance the PL with respect to emission color and intensity. Strong PL combined with its resorbable nature are essential for use of PSi particles in bioimaging[4], in particular, time-gated PL imaging[44] and as a self-reporting material in drug delivery[45, 46] and smart bandages[47] for which PSi is particularly well suited.

In this report we concentrate on using non-luminescent pulverized anodized wafers as the starting material for the formation of a luminescent hierarchical PSi powder that contains tortuous 2–4 nm pores within the ~15 nm pores produced by anodization. We call this hierarchical form of PSi ReEtched anodized porous silicon or RaPSi. We demonstrate that nanoparticles created by ball milling of RaPSi can be chemically passivated *via* hydrosilylation. This passivated material retains its visible photoluminescence (PL) – excited either with one ultraviolet/visible photon or two IR photons – for days in a simulated biological fluid. The long lifetime of the PL means that these particles are particularly well-suited for time-gated PL measurements using either one-photon nanosecond-pulsed excitation or two-photon femtosecond-pulsed excitation, the latter of which exhibits better spatial resolution and deeper tissue imaging.[48] We also demonstrate that ReEtching can introduce luminescence centers into other initially non-luminescent porous silicon-comprising powders, *e.g.* magnesiothermically reduced silica.

Results and Discussion

We have previously reported[31] that ReEtching of metallurgical grade powder produces fully porosified particles with specific surface area (SSA) that can exceed 400 m^2/g. The particles contain tortuous predominantly 3–4 nm pores. Nonetheless, the pore walls are found to be crystalline and sufficiently small to support visible photoluminescence (PL). The broad PL peak is initially centered at ~545 nm and then redshifts to ~600 nm after prolonged air exposure. The PL behavior is consistent with effects of quantum confinement, which is subsequently influenced by the presence of surface oxygen.[49, 50]

In this study, we expand upon these results to demonstrate that the parameters of ReEtching can be varied to systematically change the PL spectrum; but also, that ReEtching of anodized powder is capable of producing hierarchically nanostructured porous silicon with tunable PL. We have used as a starting material a powder made by pulverization of PSi, prepared by electrochemically anodizing high purity Si(100) wafers. After pulverization and sieving of the freestanding porous film, a powder of <75 μm particles was characterized by nitrogen sorption as mesoporous. As the earlier results showed the etching rate in the VO^{2+} initiated process to be dependent on the available area and the quality of the crystalline structure of the precursor Si material,[31] the ReEtch process conditions were adapted to the use of an initially high surface area, hydrophobic and defect-rich silicon. Aiming for milder reaction conditions, we opted to keep the amount of the primary oxidant (V_2O_5) low, settling for a concentration of 10 mM and using 120 min as the duration of the process to accommodate a slow injection rate of the regenerative, secondary oxidant (H_2O_2). The observed increase in the SSA and porosity of the ReEtched metallurgical grade powders when partially replacing water used in diluting the etchant with AcOH provided a twofold advantage by decreasing the amount of foaming occurring during the reaction, and also enabling efficient wetting of the particle surface. To facilitate the wetting of the anodized PSi, we increased the amount of AcOH to replace 75 % of the water, resulting in very little foaming during the etching.

The ReEtch process is controlled by the amount of oxidants added to the etchant, and with the very limited oxovanadium species available in the etchant, the amount of injected H_2O_2 can be used to control the outcome of the etching. Using this approach, we prepared a series of eight RaPSi samples, and monitored the effect of increasing oxidant to available silicon ratio (n_{Ox}/n_{Si}) to the mass loss ratio (MLR), defined as MLR = 1 – *yield* = 1 – (m_{RaPSi}/m_{PSi}). By selecting the oxidant-silicon ratio to cover a broad range from sub- to superstoichiometric, the structure of the resulting RaPSi could be tuned. Figure 1 shows the behavior of the observed MLR to the etchant composition. Progressively incrementing the total amount of injected H_2O_2 into the etchant resulted in larger mass loss. However, the use of superstoichiometric amounts of oxidant did not result in the complete loss of the RaPSi. This may be due to the self-limiting nature of the etching process, which is engendered by the hole injection rate of the oxovanadium species decreasing sharply as the Si crystallite size drops below 5 nm.[51]

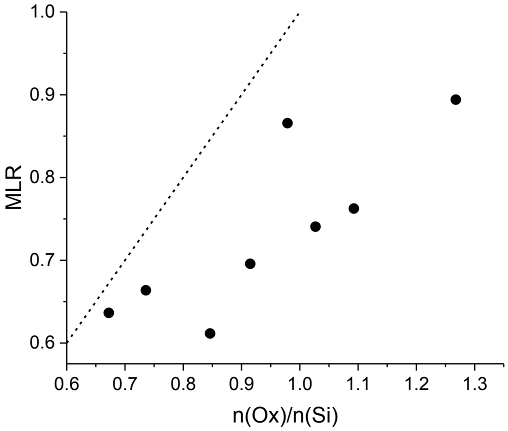

Figure 1. Observed mass loss ratio (MLR) to the selected amount of oxidants available during the ReEtch process. The dashed line shows a stoichiometric silicon dissolution in the etchant.

Structurally, the effects of the ReEtch process are profound, as indicated by N_2 sorption analysis. Table 1 lists the calculated surface areas and pore volumes of the RaPSi samples. With the lowest added oxidant amount, ca. 65 % of the silicon in the initial PSi is etched. This results in a considerable increase in the calculated SSA to over 700 m$_2$/g and porosities of over 80 %. At superstoichiometric conditions, areas of over 1000 m$_2$/g could be reached.

Table 1. The etchant composition, specific surface area and total pore volume.

Sample	$n_{\mathrm{Ox}}/n_{\mathrm{Si}}$	SSA (m$_2$/g)	Pore volume (cm$_3$/g, STP)
Initial PSi	--	307 ± 3	1.20 ± 0.01
1	0.67	723 ± 2	1.86 ± 0.03
2	0.74	761 ± 15	1.73 ± 0.01
3	0.85	780 ± 10	1.91 ± 0.02
4	0.92	925 ± 1	1.64 ± 0.03
5	0.98	961 ± 4	1.49 ± 0.01
6	1.03	1056 ± 6	1.32 ± 0.01
7	1.09	1078 ± 5	1.19 ± 0.01
8	1.27	50 ± 3	0.09 ± 0.01

Changes in the pore morphology of the RaPSi samples were evaluated with electron microscopy and pore size distribution calculations. As shown in Figure 2 and Figure S1 in Supporting Information (SI), the ReEtching does not alter the gross pore structure of the initial anodized PSi. The exposed view from the side of a particle on its pore morphology indicates that the RaPSi particles have retained their characteristic fir-tree-like pores. In FIB cut slices through a RaPSi particle, the cross-sectional view confirms this, and suggests in fact a higher density of pores after ReEtching, as shown, for example, in micrographs S2.1–S2.4 found in the SI. These observations are supported by the N$_2$ sorption isotherms (Figure S3). The isotherm shapes after ReEtching gradually transform from a type IV isotherm with an H2 hysteresis loop, typical for mesoporous materials, into an amalgamation of H2 and H4 loops.[52] This is also observed in the pore size distribution of the RaPSi samples when compared to the initial material, as seen in Figure 3. The data confirms the formation of a hierarchical pore structure as the result of ReEtching, which could be considered as type II hierarchy according to the nomenclature of Schwieger *et al.*[53] The main pores, formed during the anodization with diameters of 10–20 nm, are increasingly accompanied by tortuous 2–4 nm pores etched into the walls, with both pore types present especially in the RaPSi samples exhibiting the highest porosities. Visualization of the smaller pores is however approaching the resolution limit of SEMs at high magnifications, and is exacerbated by the high resistivity typical for PSi samples.

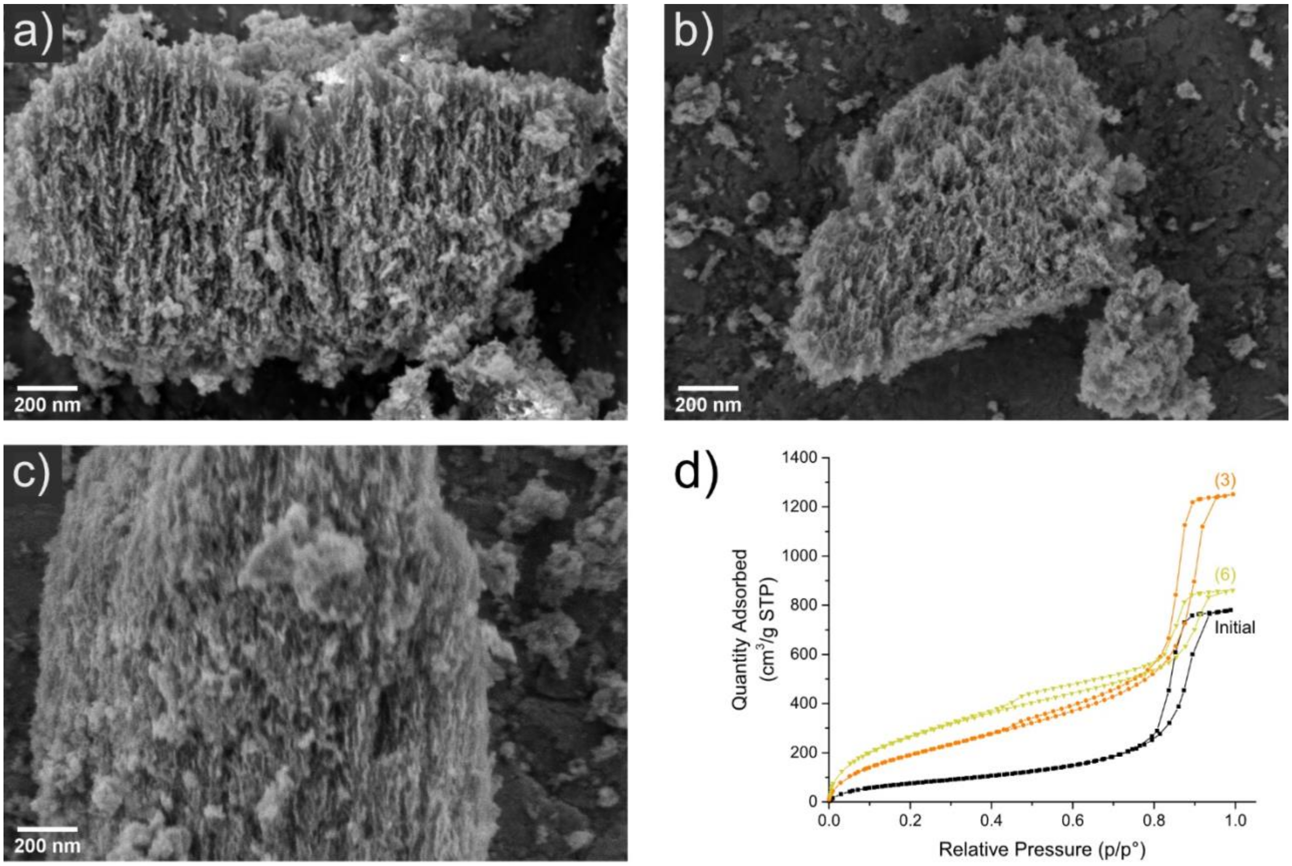

Figure 2. Secondary electron micrographs of the initial anodized PSi (a) and RaPSi samples **3** (b) and **6** (c) with the corresponding N_2 adsorption/desorption isotherms (d).

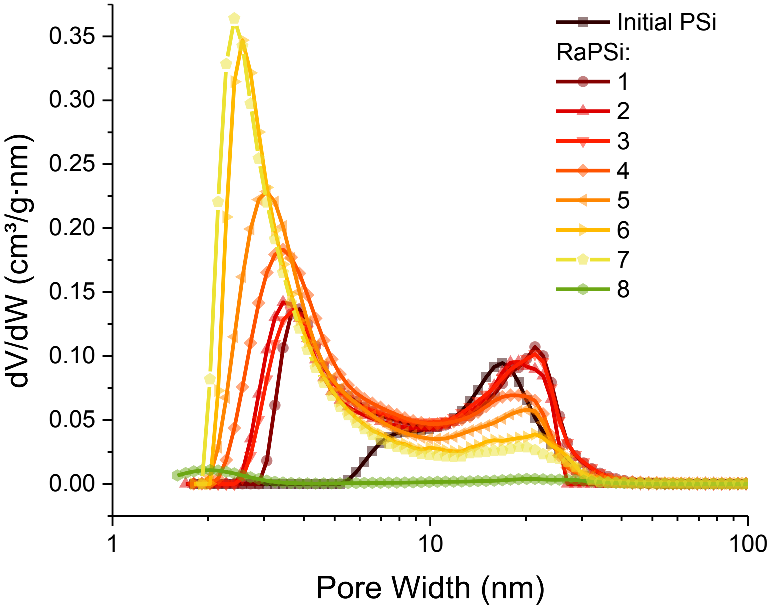

Figure 3. Pore size distributions of the initial anodized PSi and the RaPSi samples **1–8**.

The details of the porous structures were further evaluated using transmission electron microscopy (TEM). Bright-field (BF) TEM images obtained from the FIB-cut slices through the anodized and Re-Etched PSi powders are shown in Figures 4(a) and 4(c), respectively. These images reveal the interconnected pores and exhibit very complicated contrast due to the overlap of the pores through the specimen thickness. Unfortunately, the hierarchical pore structure in the RaPSi powders is not clearly revealed in such images, either. The $[1\bar{1}1]$ zone-axis selected area diffraction patterns (SADPs) in Figures 4(b) and 4(d) indicate that both the anodized and RaPSi powders are single-crystalline. Attempts have been made to mill the FIB-cut slices further to obtain thinner TEM specimens, so that better image contrast could be achieved by minimizing the effects of through-thickness pore overlapping to resolve the hierarchical pore structures. However, such attempts were unsuccessful because severe amorphization occurred in the thinnest sections due to ion beam damage.

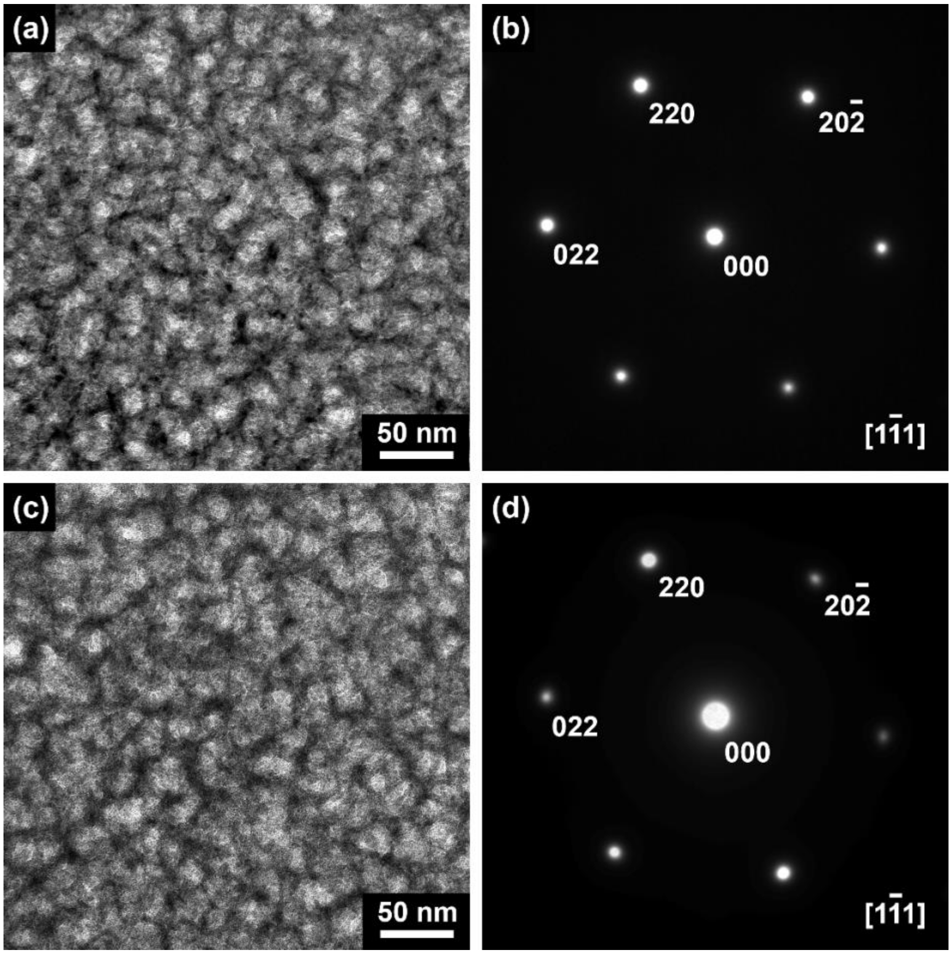

Figure 4. Examples of TEM data obtained from FIB-cut slices through porous Si powders: (a) and (c) BF TEM images of anodized PSi and RaPSi, respectively; (b) and (d) SADPs obtained from the region in (a) and (c), respectively. The patterns are presented at the same camera length.

Possibly the most striking difference in the properties of the PSi after ReEtching was the transformation of the non-photoluminescent anodized material into a luminescent hierarchical form of PSi. We have found that the PL spectrum can be tuned in response to etching conditions. We observed a general trend that greater mass loss correlated with higher specific surface area and, initially, bluer emission. This trend is shown in Figure 5, with the non-weighted intensities of each sample presented in Figure S4 and the emission peak wavelengths and widths listed in Table

S1. However, as the specific surface area exceeded 800 m^2/g, the effects of drying-induced pore collapse became ever more severe. While the SSA grew to values well over 1000 m^2/g, the corresponding total pore volume simultaneously exhibited considerable reduction, visible also in the pore size distribution. The structural collapse occurring when exceeding 80 % porosity was corroborated by powder X-ray diffraction (XRD). The diffraction patterns observed from the RaPSi powders emitting red and orange PL exhibited sharp reflexes with gradually broadening peaks compared to the as-anodized PSi, as shown in Figure 6. However, with the yellow and green emitting samples a broad halo at lower angles began to appear indicating collapsing pore structure accompanied by amorphization and possible oxidation of the RaPSi. This is most evident with the green emitting sample 8, as the SSA and pore volume are reduced to a fraction of the initial values.

The pore collapse is the result of capillary forces. While the forces may also be produced by H_2 bubble formation during etching, the preponderance of the damage likely occurred during drying; hence, we implemented a successive washing procedure, gradually replacing the aqueous etchant with ethanol and finally drying the particles from pentane. However, implementation of critical point drying would facilitate even less damage and, thus, access to higher specific surface areas and porosities.[50, 54]

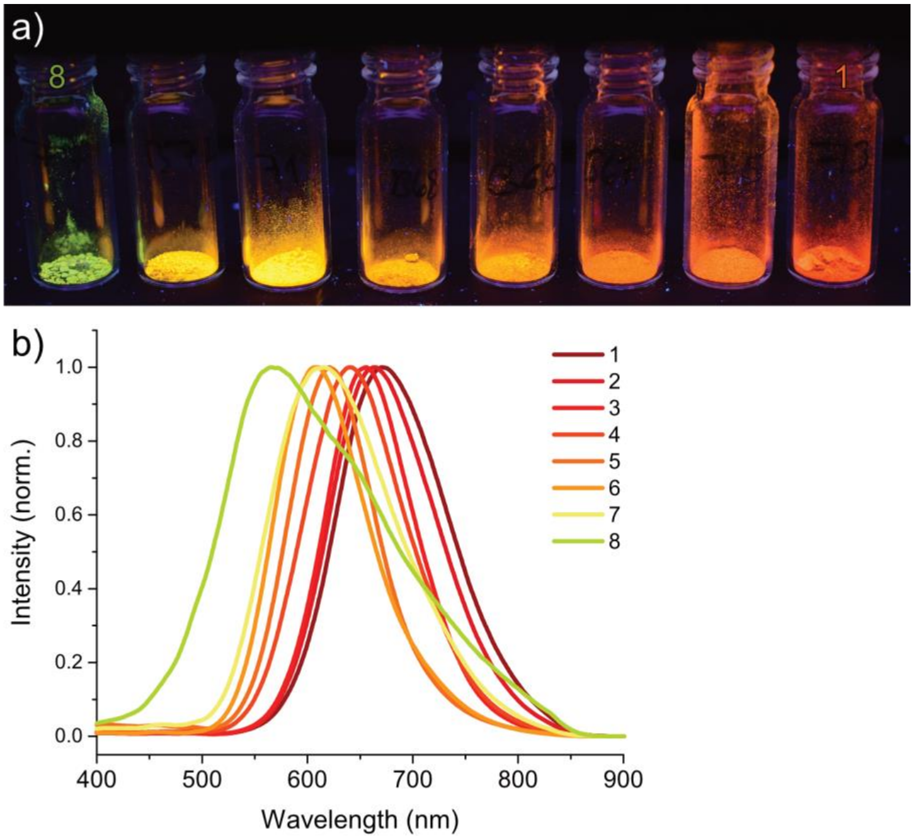

Figure 5. a) Photograph of the RaPSi samples taken with a DSLR camera using 5 s exposure time, under excitation with a handheld UV lamp at 365 nm. b) Photoluminescence spectra of the RaPSi samples excited at 325 nm. The PL peak shifts progressively towards blue with increasing mass loss ratio.

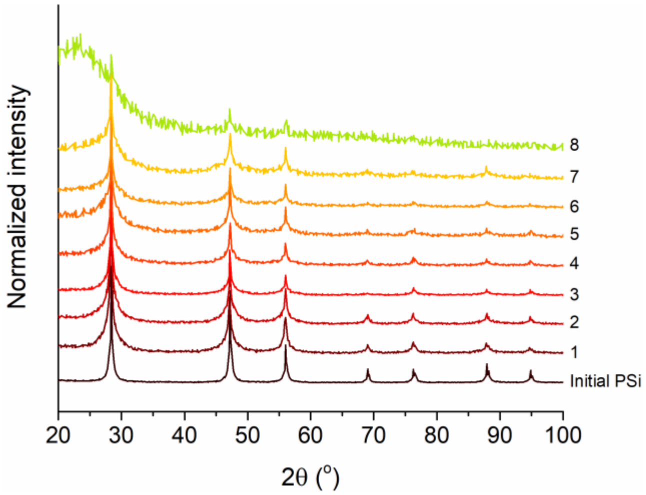

Figure 6. Powder XRD diffractograms of the anodized PSi and RaPSi samples. The intensities have been normalized and the diffractograms are vertically shifted for clarity.

An important advantage of the ReEtch process in the production of photoluminescent PSi while still retaining its mesoporous character, is the hydride-terminated surface, available for different chemical functionalizations. As the PL spectra of the particles tended to show a redshift in response to the slow oxidation of the surfaces in ambient conditions, chemical passivation can be used to mitigate this behavior. An effective method for passivating the PSi surface while providing a route to further chemical modifications is hydrosilylation. As the RaPSi particles remain hydrogen terminated after ReEtching, we selected a RaPSi batch with red-orange PL emission for further functionalization experiments. To demonstrate the suitability of the ReEtch process for the production of photoluminescent PSi nanoparticles for biomedical applications, we utilized thermal hydrosilylation in neat 10-undecylenic acid to passivate the surface against oxidation and to provide a terminal carboxylic acid group, suitable for conjugating biomolecules, such as peptides through a simple crosslinking chemistry (Figure S5). The hydrosilylated COOH-RaPSi particles retained their photoluminescence and displayed only a slight redshift of ~20 nm compared to the bare RaPSi (Figure S6).

Particularly important for the use of hierarchically structured Si in drug delivery and bio-imaging is the fabrication of nanoparticles. With the passivated high porosity COOH-RaPSi samples, we observed in the subsequent mechanical ball milling that the yield of nanoparticles could be increased closer to 40% even without systematic optimization of the process. As a high yield of nanoparticles is paramount when working with top-down fabricated material, further studies on improving the yield through more suitable design[55] of the anodized PSi may be beneficial. After milling, the final size selection of the nanoparticles was done with centrifugation. From 100 mg of COOH-RaPSi microparticles milled, we obtained nearly 40 mg of nanoparticles, having a hydrodynamic diameter of approximately 220 ± 8 nm with a PdI of 0.12 according to the DLS measurements, with the nanoparticles appearing to have retained their pore morphology and crystallinity (Figure S7).

Before more intricate testing, the stability of the COOH-RaPSi nanoparticles in a simulated biological environment was tested. Figure 7 demonstrates that when immersed in PBS buffers set to pH 7.4 and 5.5 at 37 °C, the nanoparticles retain their photoluminescence over the course of several days.

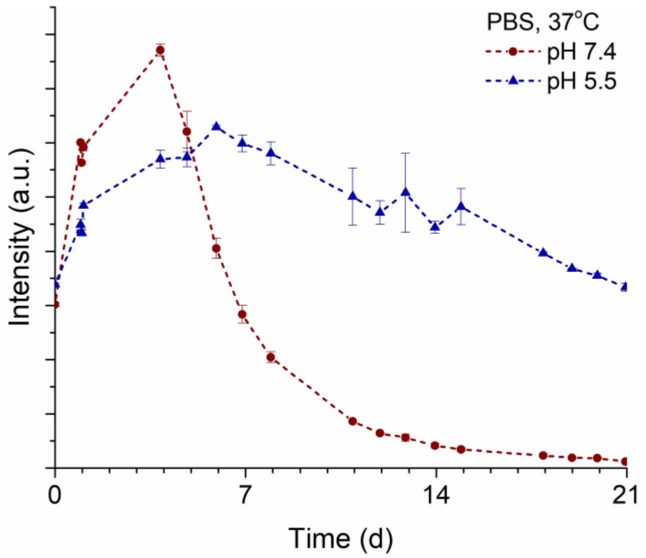

Figure 7. Stability of the photoluminescence intensity of COOH-RaPSi nanoparticles immersed into PBS buffers with pH 7.4 and 5.5 at 37 °C for three weeks. The hydrosilylation stabilizes the visible photoluminescence such that the strong red PL at 650 nm can be observed over the course of days when exposed to neutral pH 7.4 buffer.

The promising PL retention characteristics of COOH-RaPSi nanoparticles means that they can be used in conjunction with dyes and affinity targeting ligands as selective probes in fluorescence imaging. In order to test both the availability of the COOH-termination and the behavior of the nanoparticles PL, RPARPAR peptide that internalizes in NRP-1-positive cells[56] was conjugated to the nanoparticles through EDC (1-ethyl-3-(3-dimethylaminopropyl)carbodiimide) activated crosslinking. NRP-1 is a cell surface pleiotropic hub receptor with essential roles in vascular biology that is overexpressed *in vivo* in angiogenic endothelial cells, tumor cells, and cells in tumor stroma and *in vitro* in many cultured cancer cells, such as PC-3, PPC-1 and Du-145 prostate cancer cells. For the cell internalization experiments, both a fluorescently labeled free peptide (FAM-RPARPAR) and non-labeled RPARPAR-functionalized nanoparticles were incubated with PPC-1 cells. After incubating the peptide-modified nanoparticles with the cells for 1 h, the accumulation of the RaPSi nanoparticles into the cells was evident with both the FAM-labeled RPARPAR peptide (Figure 8a), and RPARPAR-functionalized NPs (Figure 8b). In the case of RPARPAR-RaPSi, the red photoluminescence indicated binding and uptake of the nanoparticles inside the PPC-1 cells. Through use of filters, both the RaPSi particles and the FAM-labeled peptide can be observed simultaneously as shown in Figure S8, due to the distinct emission maxima of the label and the particles indicating that covalent conjugation of a dye or cell internalization do not disturb or alter the initial PL properties of the RaPSi nanoparticles

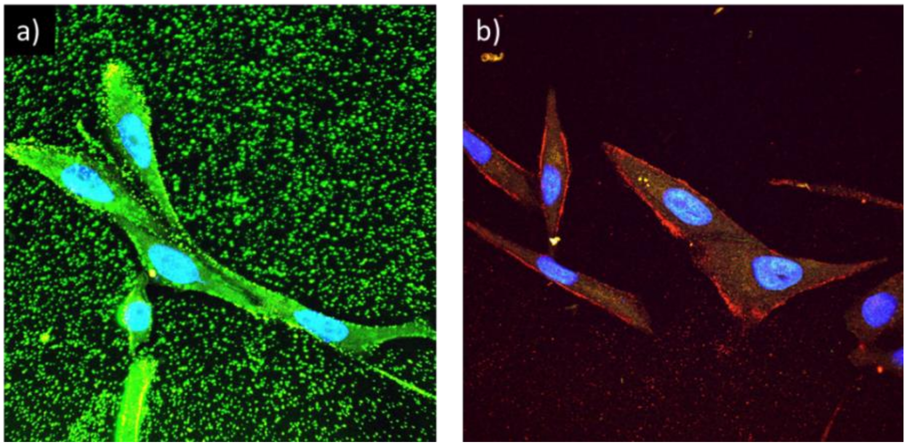

Figure 8. Confocal microscopy images of PPC-1 cells incubated with FAM-RPARPAR modified (a) and RPARPAR modified (b) COOH-RaPSi nanoparticles. Blue: DAPI-stained cell nucleus, Green: FAM, Red: RaPSi.

The application of two-photon fluorescence imaging for obtaining higher spatial resolution, contrast and the suppression of tissue autofluorescence has received significant interest.[48, 57] In this regard, we tested the excitation of the COOH-RaPSi particles with near-infrared photons of different wavelengths up to 900 nm, with the results indicating an excitation wavelength of ca. 800 nm to be most optimal for the particles used in this experiment (Figure S9). When used for excitation of the RaPSi particles internalized into the PPC-1 cells, the two-photon excitation provides comparable PL signal to the normal excitation, as shown in Figure 9.

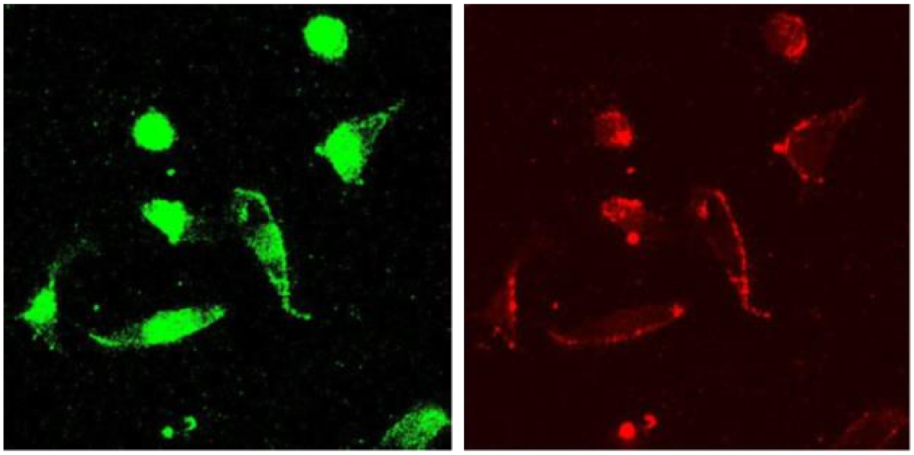

Figure 9. Confocal microscopy images of PPC-1 cells incubated with FAM-RPARPAR modified COOH-RaPSi nanoparticles. The green signal is obtained from the FAM-label of the peptide, while the red signal is emission of the COOH-RaPSi nanoparticles excited with two-photon absorption.

With the apparent ease of fabricating luminescent PSi from what was initially a non-luminescent porous powder, we also decided to test whether the ReEtch process can be extended to utilize PSi that could be derived from natural silica containing sources or from synthetic silica precursor through magnesiothermic reduction. Despite the considerable amount of silicon oxides remaining in the Mg-reduced material, a comparably low surface area according to N_2 sorption (70 m^2/g) DaviSil-based PSi powder[58] showed also the emergence of brighter photoluminescence and structural changes as shown in Figures S10.1 and S10.2. This proof-of-concept test demonstrates the capability of replacing, *e.g.*, anodized silicon with a cheaper, but still porous alternative as the feedstock material, and points toward a promising path for further studies.

Conclusion

Regenerative electroless etching (ReEtching) produces porous silicon (PSi) with tortuous, roughly 4 nm pores not only in metallurgical grade Si powder, but also powdered anodized PSi and magnesiothermically reduced silica. The strong visible/near IR photoluminescence of this material can be stabilized by hydrosilylation such that it is stable for days in phosphate buffered saline solutions (PBS). The ability of the ReEtch process to form nanostructures in virtually any silicon precursor material provides an alternative tool for hierarchical structural control. ReEtching can be used to increase the specific surface area of the initial material manifold, as well as its porosity. Even more notably, the process generates material that exhibits bright, visible photoluminescence (PL) with the apparent PL color tunable from red to green through selection of the ReEtching parameters. As the gross structural properties of the initial material are retained, such as a component of the pore size distribution, its crystallinity and hydrogen-terminated surfaces, the method allows easy fabrication of bulk quantities of hydrolytically relatively stable, luminescent porous silicon nanoparticles.

Experimental

Fabrication of Porous Silicon (PSi)

Porous Si samples have been made with reagents from multiple sources, *e.g.*, V_2O_5 (Fisher certified grade), HF (40% and 48%, Merck KGaA), H_2O_2 (35%, VWR) and glacial acetic acid (AcOH; Merck KGaA), ethanol (EtOH; 99.5%, Altia) and *n*-pentane (Merck KGaA), Si wafers (Siegert Wafer GmbH) and magnesiothermically reduced DaviSil LC250.

For anodization, p_{+}-type boron-doped, 100 mm Si(100) wafers with a resistivity of 0.01–0.02 Ω cm were used. The etching was conducted using an electrolyte with a 1:1 (vol.) ratio of HF(40%) and ethanol with a constant current density of 50 mA/cm$_2$. After the formation of ca. 90 µm thick porous layer, this was lifted off as a free-standing film by abruptly increasing the current density to over 250 mA/cm^2. The films were then ball-milled and sieved to obtain PSi microparticles with size < 75 µm. The DaviSil-based powder had been reduced into PSi utilizing the process described previously.[58] Briefly, the SiO_2-Mg powder blend (1:2 molar ratio) had been heat treated for 2 h at 700°C under Ar atmosphere and leached in 37% HCl in order to remove the remnant Mg phases.

The ReEtch process for the anodized and Mg-reduced PSi powders was conducted in plastic beakers placed in an ice/water bath, with the etchant continuously agitated with magnetic stirrer and sparged with Ar. The composition of the etchant was a volumetric ratio of 4:3:1 of HF (48%), AcOH and H_2O, with 10 mM primary oxidant (V_2O_5) concentration. The secondary oxidant (H_2O_2) was added gradually over the course of the process using a digital syringe pump (NE-500, New Era Pump Systems). Prior to the etching, half of the required HF was used to dissolve the primary oxidant. The remaining HF was mixed with the AcOH and H_2O.

In a typical scenario, 500 mg of anodized PSi powder was suspended into the HF:AcOH:H_2O solution and chilled to 0 °C under constant stirring and Ar sparging. The etching was started by adding the dissolved V_2O_5 solution into the mixture. After 5 minutes of etching, the gradual addition of H_2O_2 was initiated. The injection rate was adjusted as such that the desired amount of H_2O_2 was added 5 min before the total etching duration of 120 min was reached.

The ReEtched, anodized PSi particles (RaPSi) were then filtered from the etchant using a pressure filtration flask and a membrane filter with a nominal pore size of 1 µm. While over the filter, the particles were rinsed with copious amounts of 200 mM aqueous HCl, EtOH and finally with *n*-pentane. The filtered sample was then removed and placed into a vacuum oven at 65 °C for 1 h.

Structural characterization

The specific surface area (SSA) and total pore volume of the PSi samples were determined with N_2 sorption measurements at –196 °C using TriStar 3000 (Micromeritics Inc.). The SSA was calculated from the adsorption isotherm using BET theory, while the pore volume was obtained from the total adsorbed amount at a relative pressure, $p/p_0 = 0.97$. The pore size distribution was estimated with calculations based on the use of a kernel function derived from the Kelvin equation using the Halsey thickness curve (Microactive 4.0, Micromeritics Inc.).

The crystalline structure of the samples was studied with XRD measurements. Powder diffractograms were obtained with a Panalytical Empyrean diffractometer in θ/θ Bragg-Brentano geometry using Cu Kα radiation with a PIXcel$_{3D}$ detector in scanning line mode.

Cross-sectional TEM specimens were prepared from PSi powders using an FEI Helios Nanolab 460F1 dual-beam focused ion beam (FIB) instrument, which is equipped with a flip-stage and a scanning transmission electron microscopy (STEM) detector for improved final thinning. Details of the FIB milling conditions were reported in our previous paper [26]. In brief, a 3-μm thick Pt layer was deposited onto the surfaces of the Si particles *in situ* to protect the underlying material from Ga^+ ion beam damage during milling. In the initial stages of the milling process, the accelerating voltage used for the ion column was 30 kV and the ion beam currents were reduced iteratively from 230 to 24 pA. During the final milling process, the accelerating voltage for the ion column was reduced to 5 kV and the ion beam current used was reduced to 15 pA to avoid excessive Ga^+ implantation and beam damage. The FIB-cut slices were first directly examined using the electron beam in the dual-beam FIB for the pore morphologies on the cross-section walls. These slices were then examined in an FEI Talos F200X S/TEM operating at an accelerating voltage of 200 kV for electron imaging and diffraction analysis. Representative scanning electron microscopy (SEM) images were taken with FEI Apreo field-emission SEM (Thermo Fisher Scientific Inc.).

Surface Functionalization

Selected RaPSi particle batches were functionalized by thermal hydrosilylation by immersing the particles into neat 10-undecylenic acid and placing them at 120 °C for 16 h, after which the excess acid was removed by washing the particles with EtOH. The functionalized microparticles were then ball milled in 10 vol-% undecylenic acid-dodecane solution into nanoparticles. The milling media was removed by centrifugation and replaced with EtOH. The size selection was done with centrifugation, and the particle size distribution was monitored with dynamic laser scattering (DLS) measurements (Zetasizer Nano ZS, Malvern Instruments). The success of the functionalization into COOH-RaPSi was verified with Fourier transform infrared (FTIR) spectroscopy using Bruker Invenio spectrometer (Bruker Optik GmbH) equipped with a PA301 photoacoustic detector (Gasera Oy).

For homing peptide functionalization, COOH-RaPSi were first incubated with NH_2-PEG(3.5k)-Maleimide and EDC for 1h, followed by washing to remove excess PEG, conjugation of in-house synthesized cys-peptide with or without 5(6)-carboxyfluorescein (FAM) label, washes, and reconstitution in PBS containing 0.05% Tween-20.

Photoluminescence spectroscopy and stability testing

The photoluminescence (PL) spectra of the PSi samples were obtained with PerkinElmer LS45 fluorescence spectrometer. For the PL measurements, dry microparticles were smeared on matte black Cinefoil (Rosco Laboratories) and placed on a sample holder. The PL spectra of the PSi nanoparticles was obtained by dispersing 30 µg/mL of nanoparticles in 10 mM phosphate buffered saline (PBS) solutions with pH of 7.4 or 5.5. For the PL stability testing, the nanoparticle dispersions were stored at 37 °C. The PL excitation wavelength for all experiments was 325 nm, with a 390 nm long pass emission filter.

Cell culturing

PPC-1 cells were from the Ruoslahti laboratory at Sanford-Burnham-Prebys Medical Discovery Institute (SBPMDI). The cells were cultivated in DMEM (Lonza, Belgium) containing 100 IU/mL of penicillin, streptomycin, and 10% of heat-inactivated fetal bovine serum (GE Healthcare, UK).

Confocal microscopy

For confocal imaging of the RaPSi nanoparticles with or without FAM-label, PPC-1 cells were seeded on glass coverslips in a 24-well plate. After 24 h, nanoparticles were added to the cells and incubated at 37ºC for 1 h. The cells were washed with PBS, fixed with 4% of paraformaldehyde in PBS pH 7.4 (PFA), co-stained with DAPI, and imaged with fluorescence confocal microscopy (Olympus FV1200MPE, Germany).

Associated content

Supporting Information. The supporting information is available free of charge on the ACS Publications website. SEM and TEM figures, N_2 isotherms, FTIR spectra, photoluminescence spectra, nanoparticle size distribution data, confocal microscopy images, 2-photon excitation efficiency images.

Author information

Corresponding Author

*ermei.makila@utu.fi

**KKolasinski@wcupa.edu

Present Addresses

† Advanced Characterization Dept., Honeywell UOP, Des Plaines, IL 60017, USA

Funding Sources

Supported by funding provided by National Science Foundation award #1825331 and Academy of Finland #277190.

Acknowledgment

TEM and FIB-SEM studies were performed using the facilities in the UConn/Thermo Fisher Scientific Center for Advanced Microscopy and Materials Analysis (CAMMA).

References

1. Santos, H. A.; Mäkilä, E.; Airaksinen, A. J.; Bimbo, L. M.; Hirvonen, J., Porous Silicon Nanoparticles for Nanomedicine: Preparation and Biomedical Applications. *Nanomedicine* **2014,** *9*, 535-554.

2. Stojanovic, V.; Cunin, F.; Durand, J. O.; Garcia, M.; Gary-Bobo, M., Potential of Porous Silicon Nanoparticles as an Emerging Platform for Cancer Theranostics. *J. Mater. Chem. B* **2016,** *4*, 7050-7059.

3. Canham, L. T.; Reeves, C. L.; Wallis, D. J.; Newey, J. P.; Houlton, M. R.; Sapsford, G. J.; Godfrey, R. E.; Loni, A.; Simons, A. J.; Cox, T. I.; Ward, M. C. L., Silicon as an Active Biomaterial. *Mater. Res. Soc. Symp. Proc.* **1997,** *452*, 579-590.

4. Park, J. H.; Gu, L.; Von Maltzahn, G.; Ruoslahti, E.; Bhatia, S. N.; Sailor, M. J., Biodegradable Luminescent Porous Silicon Nanoparticles for *In Vivo* Applications. *Nature Mater.* **2009,** *8*, 331-336.

5. Henstock, J. R.; Canham, L. T.; Anderson, S. I., Silicon: The Evolution of its Use in Biomaterials. *Acta Biomaterialia* **2015,** *11*, 17-26.

6. Shahbazi, M.-A.; Hamidi, M.; Mäkilä, E. M.; Zhang, H.; Almeida, P. V.; Kaasalainen, M.; Salonen, J. J.; Hirvonen, J. T.; Santos, H. A., The Mechanisms of Surface Chemistry Effects of Mesoporous Silicon Nanoparticles on Immunotoxicity and Biocompatibility. *Biomaterials* **2013,** *34*, 7776-7789.

7. Fan, D.; Akkaraju, G. R.; Couch, E. F.; Canham, L. T.; Coffer, J. L., The Role of Nanostructured Mesoporous Silicon in Discriminating *In Vitro* Calcification for Electrospun Composite Tissue Engineering Scaffolds. *Nanoscale* **2011,** *3*, 354-361.

8. Jarvis, K. L.; Barnes, T. J.; Prestidge, C. A., Thermal Oxidation for Controlling Protein Interactions with Porous Silicon. *Langmuir* **2010,** *26*, 14316-14322.

9. Buriak, J. M., Illuminating Silicon Surface Hydrosilylation: an Unexpected Plurality of Mechanisms. *Chem. Mater.* **2014,** *26*, 763-772.

10. Salonen, J.; Mäkilä, E., Thermally Carbonized Porous Silicon and its Recent Applications. *Adv. Mater.* **2018,** *30*, 1703819.

11. Li, Y. Y.; Cunin, F.; Link, J. R.; Gao, T.; Betts, R. E.; Reiver, S. H.; Chin, V.; Bhatia, S. N.; Sailor, M. J., Polymer Replicas of Photonic Porous Silicon for Sensing and Drug Delivery Applications. *Science* **2003,** *299*, 2045-2047.

12. Bimbo, L. M.; Mäkilä, E.; Raula, J.; Laaksonen, T.; Laaksonen, P.; Strommer, K.; Kauppinen, E. I.; Salonen, J.; Linder, M. B.; Hirvonen, J.; Santos, H. A., Functional Hydrophobin-

Coating of Thermally Hydrocarbonized Porous Silicon Microparticles. *Biomaterials* **2011,** *32*, 9089-9099.

13. Tsang, C. K.; Kelly, T. L.; Sailor, M. J.; Li, Y. Y., Highly Stable Porous Silicon-Carbon Composites as Label-Free Optical Biosensors. *ACS Nano* **2012,** *6*, 10546-10554.

14. Herranz-Blanco, B.; Arriaga, L. R.; Mäkilä, E.; Correia, A.; Shrestha, N.; Mirza, S.; Weitz, D. A.; Salonen, J.; Hirvonen, J.; Santos, H. A., Microfluidic Assembly of Multistage Porous Silicon-Lipid Vesicles for Controlled Drug Release. *Lab Chip* **2014,** *14*, 1083-1086.

15. Liu, D.; Herranz-Blanco, B.; Mäkilä, E.; Arriaga, L. R.; Mirza, S.; Weitz, D. A.; Sandler, N.; Salonen, J.; Hirvonen, J.; Santos, H. A., Microfluidic Templated Mesoporous Silicon-Solid Lipid Microcomposites for Sustained Drug Delivery. *ACS Appl. Mater. Interfaces* **2013,** *5*, 12127-12134.

16. Zhang, H.; Liu, D.; Shahbazi, M.-A.; Mäkilä, E.; Herranz-Blanco, B.; Salonen, J.; Hirvonen, J.; Santos, H. A., Fabrication of A Multifunctional Nano-in-Micro Drug Delivery Platform by Microfluidic Templated Encapsulation of Porous Silicon in Polymer Matrix. *Adv. Mater.* **2014,** *26*, 4497-4503.

17. Liu, D.; Zhang, H.; Mäkilä, E.; Fan, J.; Herranz-Blanco, B.; Wang, C.-F.; Rosa, R.; Ribeiro, A. J.; Salonen, J.; Hirvonen, J.; Santos, H. A., Microfluidic Assisted One-Step Fabrication of Porous Silicon@Acetalated Dextran Nanocomposites for Precisely Controlled Combination Chemotherapy. *Biomaterials* **2015,** *39*, 249-259.

18. Salonen, J.; Laitinen, L.; Kaukonen, A. M.; Tuura, J.; Björkqvist, M.; Heikkilä, T.; Vähä-Heikkilä, K.; Hirvonen, J.; Lehto, V. P., Mesoporous Silicon Microparticles for Oral Drug Delivery: Loading and Release of Five Model Drugs. *J. Controlled Release* **2005,** *108*, 362-374.

19. Salonen, J.; Kaukonen, A. M.; Hirvonen, J.; Lehto, V.-P., Mesoporous Silicon in Drug Delivery Applications. *J. Pharm. Sci.* **2008,** *97*, 632-653.

20. Kilpeläinen, M.; Riikonen, J.; Vlasova, M. A.; Huotari, A.; Lehto, V. P.; Salonen, J.; Herzig, K. H.; Järvinen, K., *In Vivo* Delivery of a Peptide, Ghrelin Antagonist, with Mesoporous Silicon Microparticles. *J. Controlled Release* **2009,** *137*, 166-170.

21. Ashley, C. E.; Carnes, E. C.; Phillips, G. K.; Padilla, D.; Durfee, P. N.; Brown, P. A.; Hanna, T. N.; Liu, J.; Phillips, B.; Carter, M. B.; Carroll, N. J.; Jiang, X.; Dunphy, D. R.; Willman, C. L.; Petsev, D. N.; Evans, D. G.; Parikh, A. N.; Chackerian, B.; Wharton, W.; Peabody, D. S.; Brinker, C. J., The Targeted Delivery of Multicomponent Cargos to Cancer Cells by Nanoporous Particle-Supported Lipid Bilayers. *Nature Mater.* **2011,** *10*, 389-397.

22. Shen, J.; Xu, R.; Mai, J.; Kim, H.-C.; Guo, X.; Qin, G.; Yang, Y.; Wolfram, J.; Mu, C.; Xia, X.; Gu, J.; Liu, X.; Mao, Z.-W.; Ferrari, M.; Shen, H., High Capacity Nanoporous Silicon Carrier for Systemic Delivery of Gene Silencing Therapeutics. *ACS Nano* **2013,** *7*, 9867-9880

23. Kang, J.; Joo, J.; Kwon, E. J.; Skalak, M.; Hussain, S.; She, Z.-G.; Ruoslahti, E.; Bhatia, S. N.; Sailor, M. J., Self-Sealing Porous Silicon-Calcium Silicate Core-Shell Nanoparticles for Targeted siRNA Delivery to The Injured Brain. *Adv. Mater.* **2016,** *28*, 7962-7969.

24. Wareing, N.; Szymanski, K.; Akkaraju, G. R.; Loni, A.; Canham, L. T.; Gonzalez-Rodriguez, R.; Coffer, J. L., *In Vitro* Gene Delivery with Large Porous Silicon Nanoparticles Fabricated Using Cost-Effective, Metal-Assisted Chemical Etching. *Small* **2017,** *13*, 1602739.

25. Liu, D.; Bimbo, L. M.; Mäkilä, E.; Villanova, F.; Kaasalainen, M.; Herranz-Blanco, B.; Caramella, C. M.; Lehto, V. P.; Salonen, J.; Herzig, K. H.; Hirvonen, J.; Santos, H. A., Co-Delivery of a Hydrophobic Small Molecule and a Hydrophilic Peptide by Porous Silicon Nanoparticles. *J. Controlled Release* **2013,** *170*, 268-278.

26. Alhmoud, H.; Delalat, B.; Elnathan, R.; Cifuentes-Rius, A.; Chaix, A.; Rogers, M.-L.; Durand, J.-O.; Voelcker, N. H., Porous Silicon Nanodiscs for Targeted Drug Delivery. *Adv. Funct. Mater.* **2015,** *25*, 1137-1145.

27. Kim, B.; Pang, H.-B.; Kang, J.; Park, J.-H.; Ruoslahti, E.; Sailor, M. J., Immunogene Therapy with Fusogenic Nanoparticles Modulates Macrophage Response to *Staphylococcus Aureus*. *Nat. Commun.* **2018,** *9*, 1969.

28. Ferreira, M. P. A.; Ranjan, S.; Correia, A. M. R.; Mäkilä, E. M.; Kinnunen, S. M.; Zhang, H.; Shahbazi, M.-A.; Almeida, P. V.; Salonen, J. J.; Ruskoaho, H. J.; Airaksinen, A. J.; Hirvonen, J. T.; Santos, H. A., *In Vitro* and *In Vivo* Assessment of Heart-Homing Porous Silicon Nanoparticles. *Biomaterials* **2016,** *94*, 93-104.

29. Cifuentes-Rius, A.; Ivask, A.; Sporleder, E.; Kaur, I.; Assan, Y.; Rao, S.; Warther, D.; Prestidge, C. A.; Durand, J.-O.; Voelcker, N. H., Dual-Action Cancer Therapy with Targeted Porous Silicon Nanovectors. *Small* **2017,** *13*, 1701201.

30. Joo, J.; Kwon, E. J.; Kang, J.; Skalak, M.; Anglin, E. J.; Mann, A. P.; Ruoslahti, E.; Bhatia, S.; Sailor, M. J., Porous Silicon-Graphene Oxide Core-Shell Nanoparticles for Targeted Delivery of siRNA to The Injured Brain. *Nanoscale Horiz.* **2016,** *1*, 407-414.

31. Kolasinski, K. W.; Gimbar, N. J.; Yu, H.; Aindow, M.; Mäkilä, E.; Salonen, J., Regenerative Electroless Etching of Silicon. *Angew. Chem., Int. Ed. Engl.* **2017,** *56*, 624-627.

32. Kolasinski, K. W., Porous Silicon Formation by Stain Etching. in *Handbook of Porous Silicon*, 2nd Ed.; Canham, L. T., Ed. Springer Verlag: Berlin, 2018; pp 39-59.

33. Kolasinski, K. W.; Gogola, J. W.; Barclay, W. B., A Test of Marcus Theory Predictions for Electroless Etching of Silicon. *J. Phys. Chem. C* **2012,** *116*, 21472–21481.

34. Limaye, S.; Subramanian, S.; Goller, B.; Diener, J.; Kovalev, D., Scaleable Synthesis Route for Silicon Nanocrystal Assemblies *Phys. Status Solidi A* **2007,** *204*, 1297-1301.

35. Chadwick, E. G.; Mogili, N. V. V.; O'Dwyer, C.; Moore, J. D.; Fletcher, J. S.; Laffir, F.; Armstrong, G.; Tanner, D. A., Compositional Characterisation of Metallurgical Grade Silicon and Porous Silicon Nanosponge Particles. *RSC Adv.* **2013,** *3*, 19393-19402.

36. Chadwick, E. G.; Beloshapkin, S.; Tanner, D. A., Microstructural Characterisation of Metallurgical Grade Porous Silicon Nanosponge Particles *J. Mater. Sci.* **2012,** *47*, 2396-2404.

37. Wang, M.; Hartman, P. S.; Loni, A.; Canham, L. T.; Coffer, J. L., Stain Etched Nanostructured Porous Silicon: The Role of Morphology on Antibacterial Drug Loading and Release. *Silicon* **2016,** *8*, 525-531.

38. Loni, A.; Barwick, D.; Batchelor, L.; Tunbridge, J.; Han, Y.; Li, Z. Y.; Canham, L. T., Extremely High Surface Area Metallurgical-Grade Porous Silicon Powder Prepared by Metal-Assisted Etching. *Electrochem. Solid State Lett.* **2011,** *14*, K25-K27.

39. Li, Y.; Pavlovsky, I. Method of Producing Silicon Nanoparticles From Stain-Etched Silicon Powder. US 2004/0166319 A1, 2004.

40. Farrell, D.; Limaye, S.; Shanthi, S. Porous Silicon Particles. US 7560085 B2, 2007.

41. Wang, C.-F.; Sarparanta, M. P.; Mäkilä, E. M.; Hyvonen, M. L. K.; Laakkonen, P. M.; Salonen, J. J.; Hirvonen, J. T.; Airaksinen, A. J.; Santos, H. A., Multifunctional Porous Silicon Nanoparticles for Cancer Theranostics. *Biomaterials* **2015,** *48*, 108-118.

42. Li, X.; Yan, C.; Wang, J.; Graff, A.; Schweizer, S. L.; Sprafke, A.; Schmidt, O. G.; Wehrspohn, R. B., Stable Silicon Anodes for Lithium-Ion Batteries Using Mesoporous Metallurgical Silicon. *Adv. Energy Mater.* **2015,** *5*, 1401556.

43. Salonen, J.; Lehto, V. P., Fabrication and Chemical Surface Modification of Mesoporous Silicon for Biomedical Applications. *Chem. Eng. J.* **2008,** *137*, 162-172.

44. Joo, J.; Liu, X. Y.; Kotamraju, V. R.; Ruoslahti, E.; Nam, Y.; Sailor, M. J., Gated Luminescence Imaging of Silicon Nanoparticles. *ACS Nano* **2015,** *9*, 6233-6241.

45. Wang, J.; Kumeria, T.; Bezem, M. T.; Wang, J.; Sailor, M. J., Self-Reporting Photoluminescent Porous Silicon Microparticles for Drug Delivery. *ACS Appl. Mater. Interfaces* **2018,** *10*, 3200-3209.

46. Jin, Y. S.; Kim, D.; Roh, H.; Kim, S.; Hussain, S.; Kang, J. Y.; Pack, C. G.; Kim, J. K.; Myung, S. J.; Ruoslahti, E.; Sailor, M. J.; Kim, S. C.; Joo, J., Tracking The Fate of Porous Silicon

Nanoparticles Delivering A Peptide Payload by Intrinsic Photoluminescence Lifetime. *Adv. Mater.* **2018,** *30*, 1802878.

47. Chen, X. S.; Wo, F. J.; Jin, Y.; Tan, J.; Lai, Y.; Wu, J. M., Drug-Porous Silicon Dual Luminescent System for Monitoring and Inhibition of Wound Infection. *ACS Nano* **2017,** *11*, 7938-7949.

48. Kim, D.; Kang, J.; Wang, T.; Ryu, H. G.; Zuidema, J. M.; Joo, J.; Kim, M.; Huh, Y.; Jung, J.; Ahn, K. H.; Kim, K. H.; Sailor, M. J., Two-Photon *In Vivo* Imaging with Porous Silicon Nanoparticles. *Adv. Mater.* **2017,** *29*, 1703309.

49. Wolkin, M. V.; Jorne, J.; Fauchet, P. M.; Allan, G.; Delerue, C., Electronic States and Luminescence in Porous Silicon Quantum Dots: The Role of Oxygen. *Phys. Rev. Lett.* **1999,** *82*, 197-200.

50. Kolasinski, K. W.; Aindow, M.; Barnard, J. C.; Ganguly, S.; Koker, L.; Wellner, A.; Palmer, R. E.; Field, C.; Hamley, P.; Poliakoff, M., on The Role of the Pore Filling Medium in Photoluminescence from Photochemically Etched Porous Silicon. *J. Appl. Phys.* **2000,** *88*, 2472-2479.

51. Kolasinski, K. W., Charge Transfer and Nanostructure Formation During Electroless Etching of Silicon. *J. Phys. Chem. C* **2010,** *114*, 22098–22105.

52. Thommes, M.; Kaneko, K.; Neimark Alexander, V.; Olivier James, P.; Rodriguez-Reinoso, F.; Rouquerol, J.; Sing Kenneth, S. W., Physisorption of Gases, with Special Reference to The Evaluation of Surface Area and Pore Size Distribution (IUPAC Technical Report). *Pure Appl. Chem.* **2015,** *87*, 1051-1069.

53. Schwieger, W.; Machoke, A. G.; Weissenberger, T.; Inayat, A.; Selvam, T.; Klumpp, M.; Inayat, A., Hierarchy Concepts: Classification and Preparation Strategies for Zeolite Containing Materials with Hierarchical Porosity. *Chem. Soc. Rev.* **2016,** *45*, 3353-3376.

54. Bellet, D.; Canham, L., Controlled Drying: The Key to Better Quality Porous Semiconductors. *Adv. Mater.* **1998,** *10*, 487-490.

55. Bimbo, L. M.; Sarparanta, M.; Santos, H. A.; Airaksinen, A. J.; Mäkilä, E.; Laaksonen, T.; Peltonen, L.; Lehto, V.-P.; Hirvonen, J.; Salonen, J., Biocompatibility of Thermally Hydrocarbonized Porous Silicon Nanoparticles and Their Biodistribution in Rats. *ACS Nano* **2010,** *4*, 3023-3032.

56. Teesalu, T.; Sugahara, K. N.; Kotamraju, V. R.; Ruoslahti, E., C-End Rule Peptides Mediate Neuropilin-1-Dependent Cell, Vascular, and Tissue Penetration. *Proc. Natl. Acad. Sci. U. S. A.* **2009,** *106*, 16157-16162.

57. Furey, B. J.; Silbaugh, D. A.; Yu, Y.; Guillaussier, A. C.; Estrada, A. D.; Stevens, C.; Maynard, J. A.; Korgel, B. A.; Downer, M. C., Measurement of Two-Photon Absorption of Silicon Nanocrystals in Colloidal Suspension for Bio-Imaging Applications. *Phys. Status Solidi B* **2018,** *255*, 1700501.

58. Batchelor, L.; Loni, A.; Canham, L. T.; Hasan, M.; Coffer, J. L., Manufacture of Mesoporous Silicon from Living Plants and Agricultural Waste: an Environmentally Friendly and Scalable Process. *Silicon* **2012,** *4*, 259-266.